PdPt Bimetal Functionalized SnO$_2$ Nanosheets: Controllable Synthesis and its Dual Selectivity for Detection of Carbon Monoxide and Methane

Gaojie Li[†], Xiaohong Wang[†], Liuming Yan[†], Yan Wang[‡], Zhanying Zhang*[§], Jiaqiang Xu*[†]

[†]NEST lab, Department of Physics, Department of Chemistry, College of Science, Shanghai University, Shanghai 200444, China

[‡]School of Safety Science and Engineering, State Key Laboratory Cultivation Base for Gas Geology and Gas Control, Henan Polytechnic University, Jiaozuo 454000, China

[§]School of Materials Science and Engineering, Cultivating Base for Key Laboratory of Environment-friendly Inorganic Materials in University of Henan Province, Henan Polytechnic University, Jiaozuo 454000, China

KEYWORDS: PdPt bimetal, SnO$_2$ nanosheets, Chemical sensitization, electronic sensitization, Carbon monoxide sensor, Methane sensor

*Corresponding author: Prof. Jiaqiang Xu, xujiaqiang@shu.edu.cn

Prof. Zhanying Zhang, zhangzy@hpu.edu.cn

Table of Contents

#Note S1 Synthesis of PdPt/SnO$_2$ composite by traditional reduction method.

100 mg SnO$_2$ NSs was dispersed into 20 mL distilled water under ultrasonication for 15 min, followed by adding 167 μL PdCl$_2$ (20 mM) and 167 μL PtCl$_2$ (20 mM) solution, and then 4 mL NaBH$_4$ (10 mM) was added dropwise under stirring for 5 min. The precipitate was separated by centrifugation, repeatedly washed with distilled water for several times, dried for 8 h at 80 °C. The calcination procedure was the same as above and the final product was labeled as1P-PdPt/SnO$_2$-B (1.0 wt%). Under the same conditions, 0.5P-PdPt/SnO$_2$-B (0.5 wt%), 1.5P-PdPt/SnO$_2$-B (1.5 wt%) and 2P-PdPt/SnO$_2$-B (2.0 wt%) were prepared by adding 83.5 μL PdCl$_2$ and 83.5 μL PtCl$_2$, 250.5 μL PdCl$_2$ and 250.5 μL PtCl$_2$, 334 μL PdCl$_2$ and 334 μL PtCl$_2$, respectively.

#Note S2 Characterization.

Crystal structure of the products was characterized by X-ray diffraction analysis (XRD, Rigaku Corp., D/max2500) by using Cu Kα radiation (40 mA, 40 kV, 6° min^{-1} from 15 to 80°). The morphologies of all the samples were observed by Transmission electron microscopy (TEM, JEOL Ltd., JEM-2100F) equipped with an energy dispersive X-ray spectroscopy (EDS), operating at 200 kV. The chemical states of the surface elements were measured by X-ray photoelectron spectroscopy (XPS, Thermo fisher scientific Ltd, ESCALAB 250Xi) by using an Al Kα monochromated (150 W, 20 eV pass energy, 500 μm spot size). The C 1s signal at 284.5 eV was used to calibrate the binding energy scale. Spectra were analyzed using Thermo Scientific Avantage 5.52 software. Photoluminescence (PL) measurements were conducted on a Hitachi RF-5301PC fluorescence spectrophotometer using a 280 nm Xe laser line as an excitation source. The composition of the PdPt bimetal was measured by the inductively coupled plasma atomic emission spectroscopy (ICP-AES, ICAP-6300) and energy dispersive spectrometer (EDS).

#Note S3 Fabrication and Response Test of the Gas Sensor

The fabrication of the gas sensor as as follows: Firstly, the prepared samples and adhesive were mixed together in an agate mortar to make a paste by grinding. Then, the paste was coated on the ceramic tube consisted of a pair of previously printed Au electrodes and Pt conducting wires (Fig S1a). Subsequently the prepared ceramic tube was sintered at 350 °C for 2 h in order to remove the adhesive and then welded onto a pedestal (Fig. S1b). The aim of heat treatment process is to remove the adhesive and forms a porous and stable gas sensing layer, which is favorable for gas diffusion and sensing. The nano morphology of the material itself do not change obviously after the teat treatment process. Ni-Cr heating wire inside the ceramic tube was used to control the operating temperature of the sensor. Finally, the obtained sensors were aged at 240 °C for 7 days to improve their stability.

The performance evaluation was performed by a WS-30A tester (Hanwei Electronics Co. Ltd., P.R. China). Fig S1c is a measuring electric circuit for the gas sensor. As shown in Fig. S1d, the operating temperature was controlled by changing the heating voltage (V_h). V_c is the voltage of the test circuit. The fan is used to accelerate the diffusion rate of gas in the test chamber. The temperature and humidity of the test chamber is measured by a temperature sensor and a humidity sensor, respectively. A stationary state gas distribution method was used for testing gas response. In this measurement, the humidity is controlled at about 40% RH, the ambient temperature is room temperature (25 °C) and the chamber temperature was 25~28 °C. Ambient humidity is controlled by the humidifier (DOROSN, CH-12T) and the dehumidifier (SEN Electric, E18). Ambient temperature is controlled by air conditioner (GREE, KFR-35GW). In the humidity test, the high humidity can be obtained by the humidifier. To obtain the desired gas concentration, injection volume of the gas could be calculated as follow:

$$V_x = V \times C \times 10^{-6} \times \frac{273 + T_r}{273 + T_c}$$

Where V_x is the injection volume (mL), V is the test chamber volume (mL), C is the gas concentration (ppm), T_r is the room temperature (°C), T_c is the chamber temperature (°C). In our study, the gases used are standard gases. The concentrations of CO and

CH$_4$ are 99.99%. The concentrations of NH$_3$ and H$_2$S are 1000 ppm (Equilibrium gas: N$_2$). The volume of test chamber is 18000 mL.

Detailed testing procedures are as follows. As shown in Fig. S1e, before the injection of the test gas, the test chamber was covered and filled with air. Keeping the fan of the measurement system working would favor the diffusion of the air. Under this working temperature, we could get the resistance of the sensor in the air (R$_a$). After the injection (the gas was immediately injected into the test chamber and mixed with air), the test chamber was still covered, meanwhile, the resistance of the sensor changed and reached a stable value several seconds later, then the resistance of the sensor in the test gas (R$_g$) was recorded. Open the test chamber, the sensor was in contact with air again, and the resistance of the sensor would return to the level before the gas injection. The gas response (*S*) of the sensor in this paper was defined as $S = R_a/R_g$ (reducing gases), where R$_a$ and R$_g$ were the resistances in air and test gas, respectively. The selectivity coefficient (*K*) of the sensor was defined as $K = S_A/S_B$, in which S_A and S_B represent the response of the sensor in different gases. The response or recovery times were expressed as the time taken for the sensor output to reach 95% of its saturation after applying or switching off the gas in a step function.

#Note S4 Sensing performance of PdPt/SnO$_2$-B composite sensors by traditional reduction method

The responses of PdPt/SnO$_2$-B sensors obtained by traditional reduction method to 50 ppm of CO and 500 ppm of CH$_4$ at different working temperature were show in Fig. S7. As shown, at low working temperature (40~160 °C), 1.5P-PdPt/SnO$_2$-B exhibited highest responses to 50 ppm of CO in comparison with other PdPt/SnO$_2$-B composites, and the responses gradually decreased with the increasing working temperature (Fig. S6a). At high working temperature (200~400 °C), 1.5P-PdPt/SnO$_2$-B and 2P-PdPt/SnO$_2$-B exhibited high response to CH$_4$. And the response of 1.5P-PdPt/SnO$_2$-B sensor to CH$_4$ is higher than that of 2P-PdPt/SnO$_2$-B at the optimum working temperature (320 °C), which can be attributed to aggregation of PdPt NPs. Therefore, it is speculated that the optimal content of PdPt bimetal is about 1.5 wt%.

<Figure. S1>
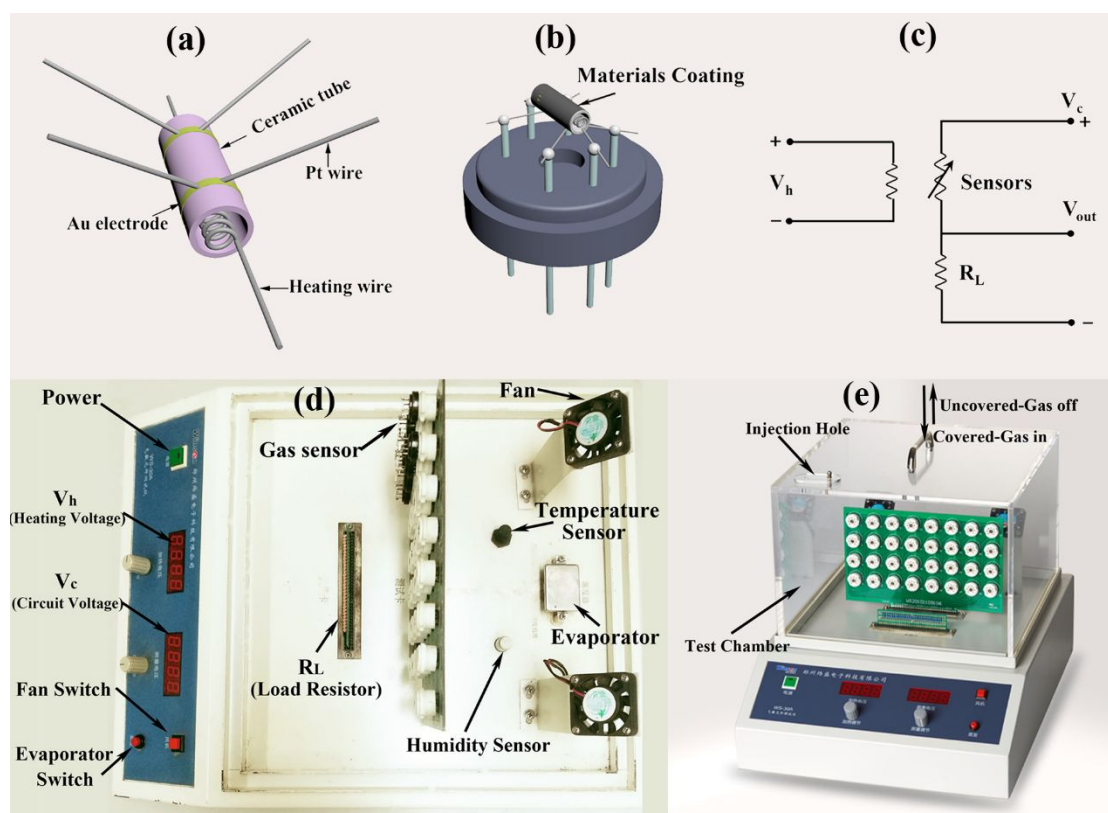
Fig. S1: Sketch of (a) the Ceramic tube structure, (b) Sensor element structure, (c) test circuit of the sensor, (d and e) photographs of gas sensing test apparatus.

<Figure. S2>
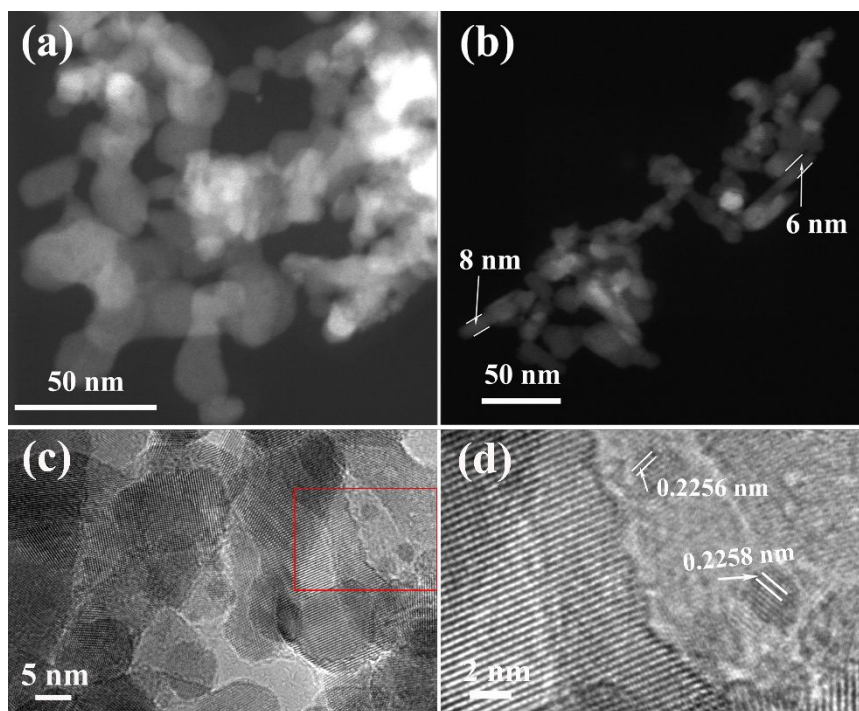
Fig. S2 (a and b) HAADF-STEM image of SnO$_2$ NSs, (c and d) HTEM images of 1P-PdPt/SnO$_2$-A.
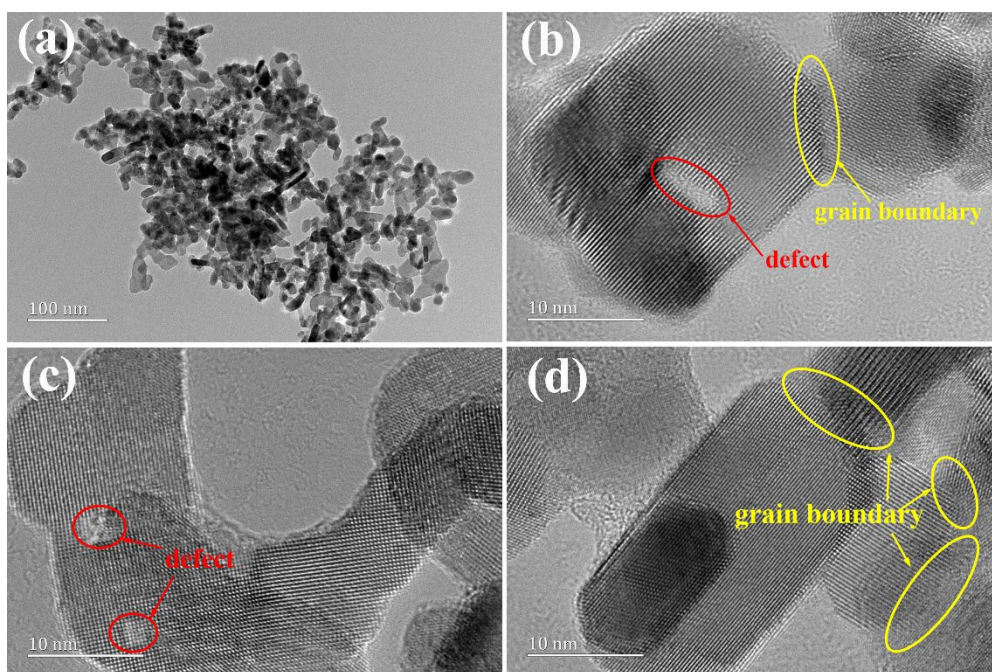
Fig. S3 (a) TEM image and (b-d) HRTEM images of pristine SnO_2 NSs.

<Figure. S4>
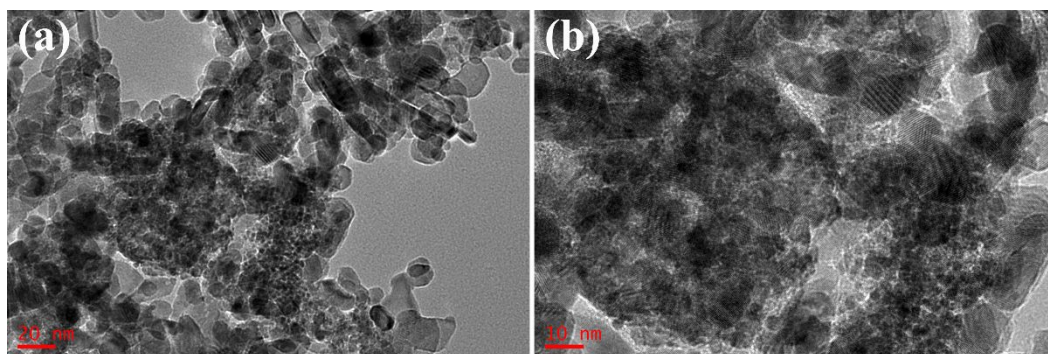
Fig. S4 TEM images of 1P-PdPt/SnO$_2$-B sample prepared by traditional reduction method using NaBH$_4$.

<Figure. S5>
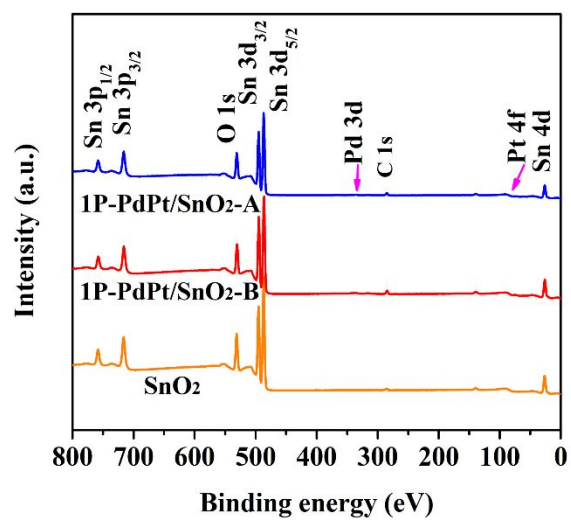
Fig. S5 Survey XPS spectra of pristine SnO_2, 1P-PdPt/SnO_2-A and 1P-PdPt/SnO_2-B.

<Figure. S6>
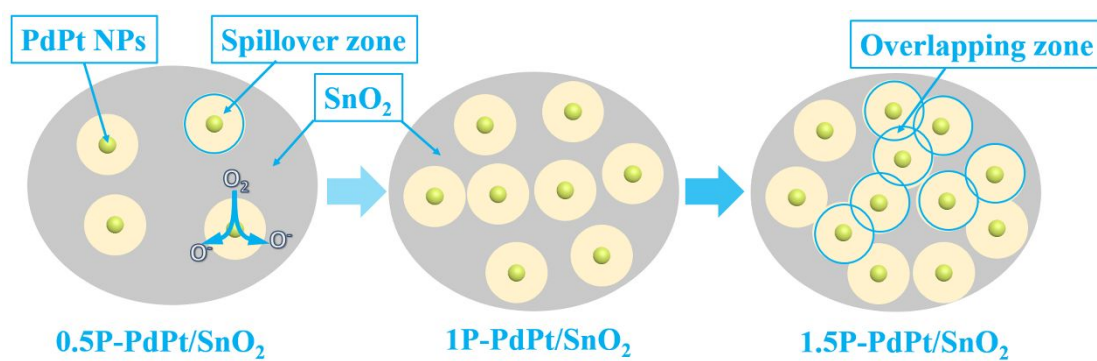
Fig. S6 The illustration of the spillover effect of noble metals.

<Figure. S7>
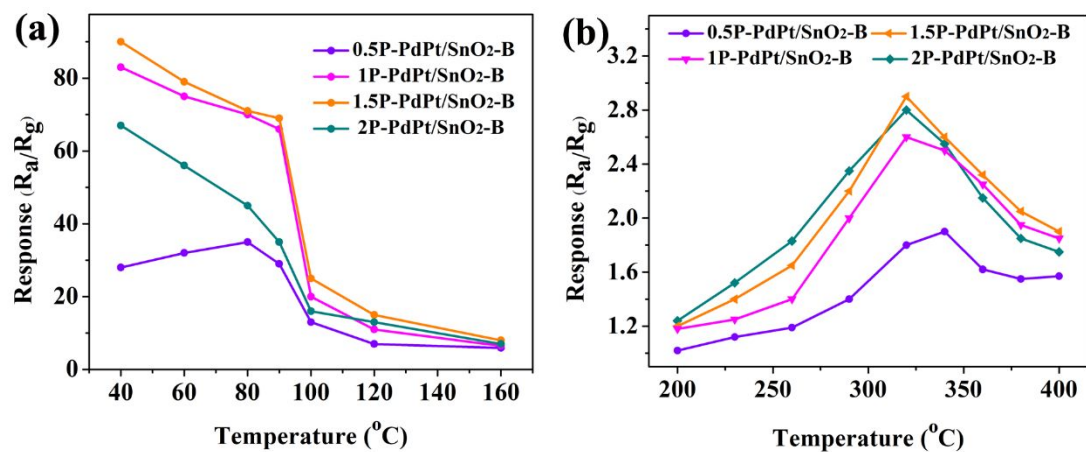
Fig. S7 The responses of the PdPt/SnO$_2$ sensors obtained by traditional reduction method to (a) 50 ppm of CO, (b) 500 ppm of CH$_4$ at different working temperature.

<Figure. S8>
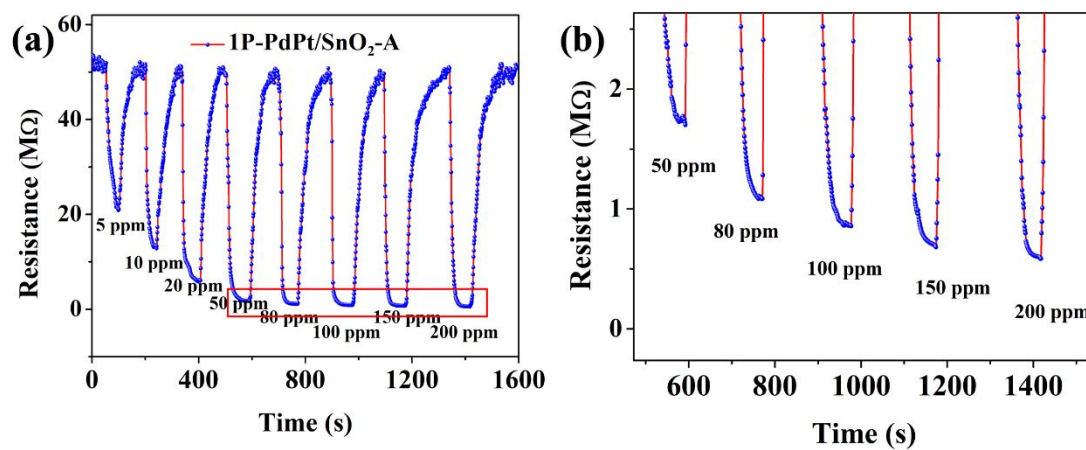
Fig. S8 (a) Dynamic responses of the 1P-PdPt/SnO$_2$-A sensor to varying
concentration of CO at 100 °C and (b) partial enlargement
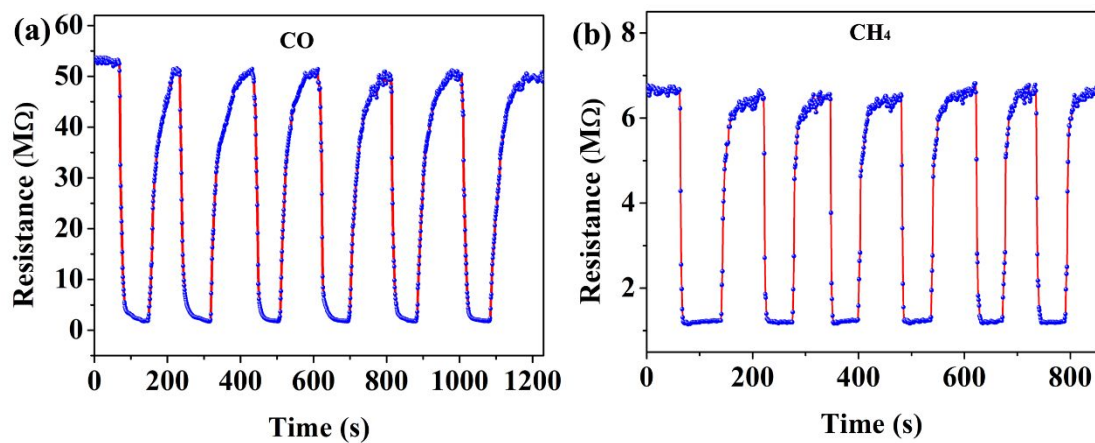
Fig. S9 Responses of 1P-PdPt/SnO$_2$-A sensor to (a) 50 ppm of CO at 100 °C and (b) 1000 ppm of CH$_4$ at 320 °C for six repeated exposure cycles.
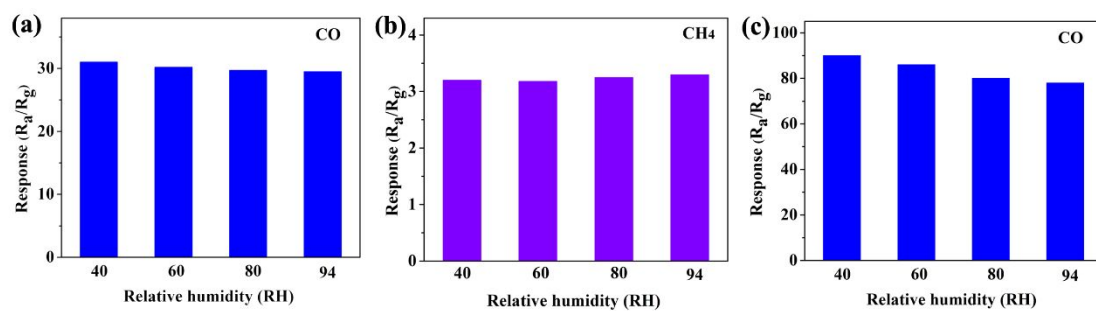
Fig. S10 The response of 1P-PdAu/SnO$_2$-A sensor to CO and CH$_4$ at different relative humidity (a) 50 ppm CO at 100 °C, (b) 500 ppm CH$_4$ at 320 °C, (c) 50 ppm CO at 90 °C.
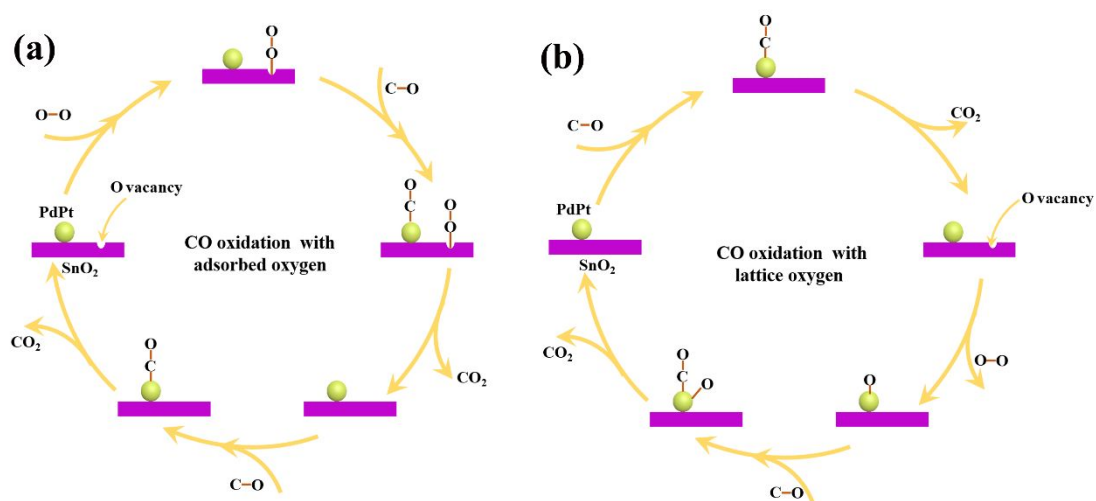
Fig. S11 Scheme of CO oxidation mechanism. CO oxidation with (a) adsorbed oxygen and (b) lattice oxygen on the surface of SnO_2.

<Figure. S12>
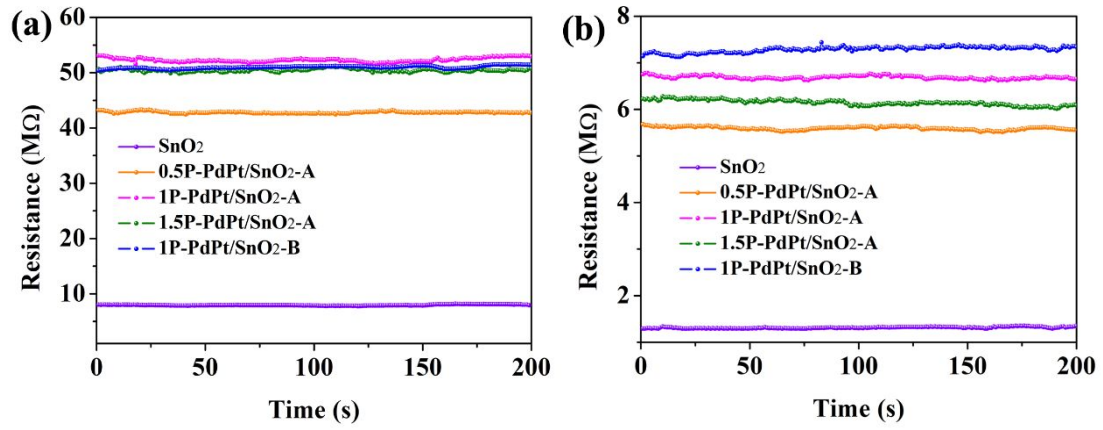
Fig. S12 Base-resistance in air of the obtained sensors at (a) 100 °C and (b) 320 °C.

Table S1 Molar ratio of Pd to Pt was measured by ICP.

Samples	Pd (mg/ml)	Pt (mg/ml)	Molar ratio of Pd to Pt
PdPt NPs	0.1105	0.1921	1.0/0.947

Table S2 The sensing performance parameters of 1P-PdPt/SnO$_2$-A sensor at different working temperature.

Sensor	Temperature	Response	Response and Recovery times	94% RH
1P-PdPt/SnO$_2$-A	90 °C	90	44/112 s	~ 13%
	95 °C	68	38/93 s	~ 10%
	100 °C	30	30/78 s	~ 3%

Table S3 The response and recovery times of the obtained sensors to 50 ppm of CO at different working temperature.

| Samples	Tem.(°C)	40	60	80	90	95	100	120	160	200	220	240	260	280	300
SnO$_2$	τ_{res} (s)									58	50	40	35	22	15
	τ_{rec} (s)									78	69	52	43	25	
1P-PdPt/SnO$_2$-A	τ_{res} (s)	115	89	68	44	38	30	18	7	3					
	τ_{rec} (s)	292	235	158	112	93	78	59	26	9					
1P-PdPt/SnO$_2$-B	τ_{res} (s)	165	118	85	55	43	35	21	8.5	3.5					
	τ_{rec} (s)	358	286	189	145	106	92	74	35	12					

Note: τ_{res} is response times. τ_{rec} is recovery times.

Table S4 The response times of the obtained samples to 1000 ppm of CH$_4$ at different working temperature.

Samples	Tem. (°C)	200	230	260	280	300	320	360	400	440
SnO$_2$	τ_{res} (s)					25	17	11	7	5
1P-PdPt/SnO$_2$-A	τ_{res} (s)	20	16	11	7		5	4	3	
1P-PdPt/SnO$_2$-B	τ_{res} (s)	26	21	15	9		7	5	3	

Note: τ_{res} is response times.

Table S5 Comparison of the sensing performance of SnO_2-based gas sensor toward CO and CH_4, respectively.

Material	Morphology	Gas	Temp. (°C)	Conc. (ppm)	Response (Ra/Rg)	Res/Rec. time (s/s)	Ref.
Pd/SnO_2	Nanowires	CO	400	1	1.8	10/7	1
Pd/SnO_2	Nanosheets	CO	125	100	7	60/150	2
Pd/SnO_2	Nanoparticles	CO	60	18	1.9	-	3
Pt/SnO_2	Nanosheets	CO	400	10	2.34	6/-	4
$PdPt/SnO_2$	Nanocrystals	CO	100	1	6.5	5/4	This work
SnO_2	Thick film	CH_4	350	1000	1.85	-/95	5
SnO_2-Ni_2O_3	Thick film	CH_4	400	200	1.27	13/28	6
Pd/SnO_2	Thick film	CH_4	220	200	1.97	38/100	7
Pt/SnO_2	Thick film	CH_4	325	5000	2.13	-	8
$PdPt/SnO_2$	Nanosheets	CH_4	320	500	3.1	5/4	This work

Table S6 The resistance of the obtained sensors in air and 50 ppm CO at different working temperature, respectively.

Sample	Resistance (MΩ)	Working temperature (°C)						
		40	60	80	90	100	120	160
SnO_2	Ra	11.2	10.7	9.6	9.0	7.8	5.9	3.6
	R_{CO}	11.2	10.7	9.6	9.0	7.8	5.4	2.8
1P-$PdPt/SnO_2$-A	Ra	99.6	82.3	70.5	63.8	52.8	42.0	45.6
	R_{CO}	0.98	0.89	0.83	0.71	1.7	2.6	5.8
1P-$PdPt/SnO_2$-B	Ra	91.8	77.9	65.2	54.1	50.9	39.7	41.8
	R_{CO}	1.1	1.1	0.93	0.82	2.5	3.6	6.4

Table S7 The resistance of the obtained sensors in air and 500 ppm CH_4 at different working temperature, respectively.

Sample	Resistance (MΩ)	Working temperature (°C)								
		200	230	260	290	320	340	360	380	400
SnO_2	Ra	3.2	2.5	3.1	1.8	1.2	1.1	0.95	1.3	1.2
	R_{CH4}	3.2	2.5	3.1	1.7	1.1	0.88	0.67	0.81	0.73
1P-$PdPt/SnO_2$-A	Ra	31.7	16.6	9.3	5.8	6.7	7.4	5.9	5.5	4.9
	R_{CH4}	27.3	12.2	5.5	2.2	2.1	2.6	2.2	2.3	2.3
1P-$PdPt/SnO_2$-B	Ra	32.9	18.8	11.6	7.9	7.3	7.8	6.7	6.5	6.3
	R_{CH4}	27.4	13.4	7.4	3.6	2.7	3.0	2.8	3.3	3.2

REFERENCES

(1) Trung, D. D.; Hoa, N. D.; Tong, P. V.; Duy, N. V.; T., D.; CHUNG; H., V.; NAGAO. Effective Decoration of Pd Nanoparticles on the Surface of SnO_2 Nanowires for Enhancement of CO Gas-sensing Performance. *J. Hazard. Mater.* **2014,** *265*, 124-132.

(2) Wang, Q.; Chen, W.; Sun, H.; Peng, S.; Wang, Y.; Lin, J.; Lu, G. Microwave Assisted Synthesis of Hierarchical Pd/SnO_2 Nanostructures for CO Gas Sensor. *Sens. Actuators, B* **2016,** *222*, 257-263.

(3) Kim, B.; Lu, Y.; Hannon, A.; Meyyappan, M.; Li, J. Low Temperature Pd/SnO_2 Sensor for Carbon Monoxide Detection. *Sens. Actuators, B* **2013,** *177*, 770-775.

(4) Chang, S. M.; Kim, HaeRyong; Graeme, A.; Drennan, J.; Lee, J.H. JongHeun. Highly Sensitive and Fast Responding CO Sensor Using SnO_2 Nanosheets. *Sens. Actuators, B* **2008,** *131*, 556-564.

(5) Chakraborty, S.; Mandal, I.; Ray, I.; Majumdar, S.; Sen, A.; Maiti, H. S. Improvement of Recovery Time of Nanostructured Tin Dioxide-based Thick Film Gas Gensors Through Surface Modification. *Sens. Actuators, B* **2007,** *127*, 554-558.

(6) Vuong, N. M.; Hieu, N. M.; Hieu, H. N.; Yi, H.; Kim, D.; Han, Y. S.; Kim, M. Ni_2O_3-decorated SnO_2 Particulate Films for Methane Gas Sensors. *Sens. Actuators, B* **2014,** *192*, 327-333.

(7) Haridas, D.; Gupta, V. Enhanced Response Characteristics of SnO_2 Thin Film Based Sensors Loaded with Pd Clusters for Methane Detection. *Sens. Actuators, B* **2012,** *166-167*, 156-164.

(8) Min, B.-K.; Choi, S.-D. Undoped and 0.1 wt% Ca-doped Pt-catalyzed SnO_2 Sensors for CH_4 Detection. *Sens. Actuators, B.* **2005,** *108*, 119-124.